Nonlinear Biasing and Redshift-Space Distortions in Lagrangian Resummation Theory and N-body Simulations

Masanori Sato(Nagoya)

with Takahiko Matsubara(Nagoya)

reference; Sato and Matsubara, arXiv:1105.5007, PRD in press.

RESCEU/DENET Summer School@Kumamoto

Introduction

- Bottom line: Baryon Acoustic Oscillations(BAOs) are expected to provide a tight constraint on the nature of dark energy, using the BAOs as a standard ruler.
- According to the dark energy task force(Albrecht+2006), BAOs are less affected by systematic effects than other techniques, such as weak lensing, Supernova, etc.
- However, to exploit the full potential of upcoming high-quality data, we have to treat the systematic effects on BAOs.
- The main systematic effects: galaxy biasing, nonlinearity, and redshift-space distortions

Motivation

- Therefore, we have to make an accurate theoretical template including a systematic effects; galaxy biasing, nonlinearity and redshift-space distortions
- We use theoretical model proposed by Matsubara(2008) (LRT) which naturally incorporate above all of systematic effects into their formalism of perturbation theory with a resummation technique via Lagrangian picture <- no fitting parameter
- Other perturbation or resummation technique with bias; Smith+(2007,2008) ,Elia+2011 using TRG, Nishimichi & Taruya (2011)->probably Nishimichi-san's talk

Why Lagrangian resummation theory?

- Problem of Eulerian bias->no physical model of Eulerian bias!
- Physical models of bias known so far is provided in Lagrangian space;
  - e.g. halo bias model, peak bias model
- LRT is suitable for handling Lagrangian bias

Lagrangian resummation theory

- Fundamental variables in Lagrangian picture is displacement field $\boldsymbol{\Psi}(\boldsymbol{q},t)$

$$\boldsymbol{\Psi}(\boldsymbol{q},t)=\boldsymbol{x}(\boldsymbol{q},t)-\boldsymbol{q}$$

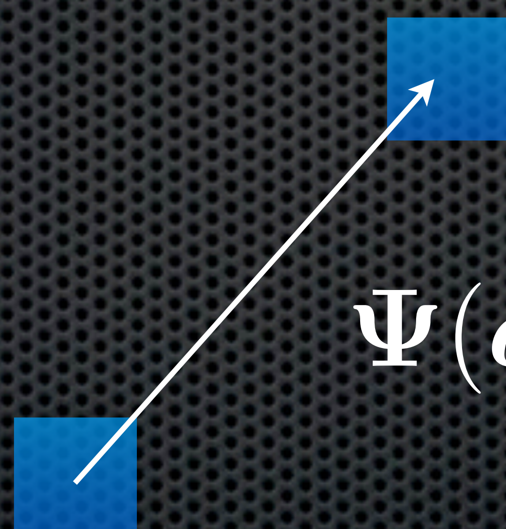

$\boldsymbol{x}(\boldsymbol{q},t)$ Eulerian final position

$\boldsymbol{\Psi}(\boldsymbol{q},t)$ displacement field

$\boldsymbol{q}$ Lagrangian initial position

Redshift-space distortions

- Redshift-space distortions are easily incorporated into LRT
- Mapping is exactly linear in Lagrangian variables

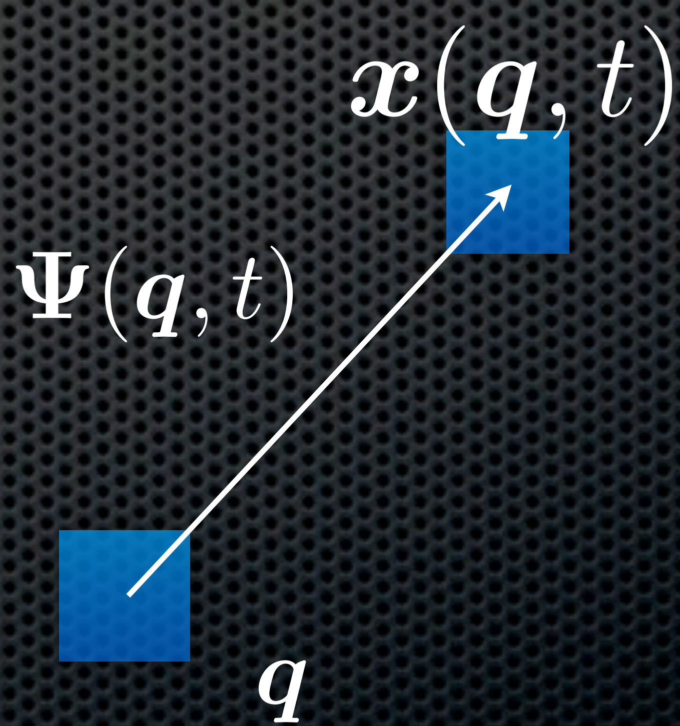

Redshift-space distortions

- Redshift-space distortions are easily incorporated into LRT
- Mapping is exactly linear in Lagrangian variables

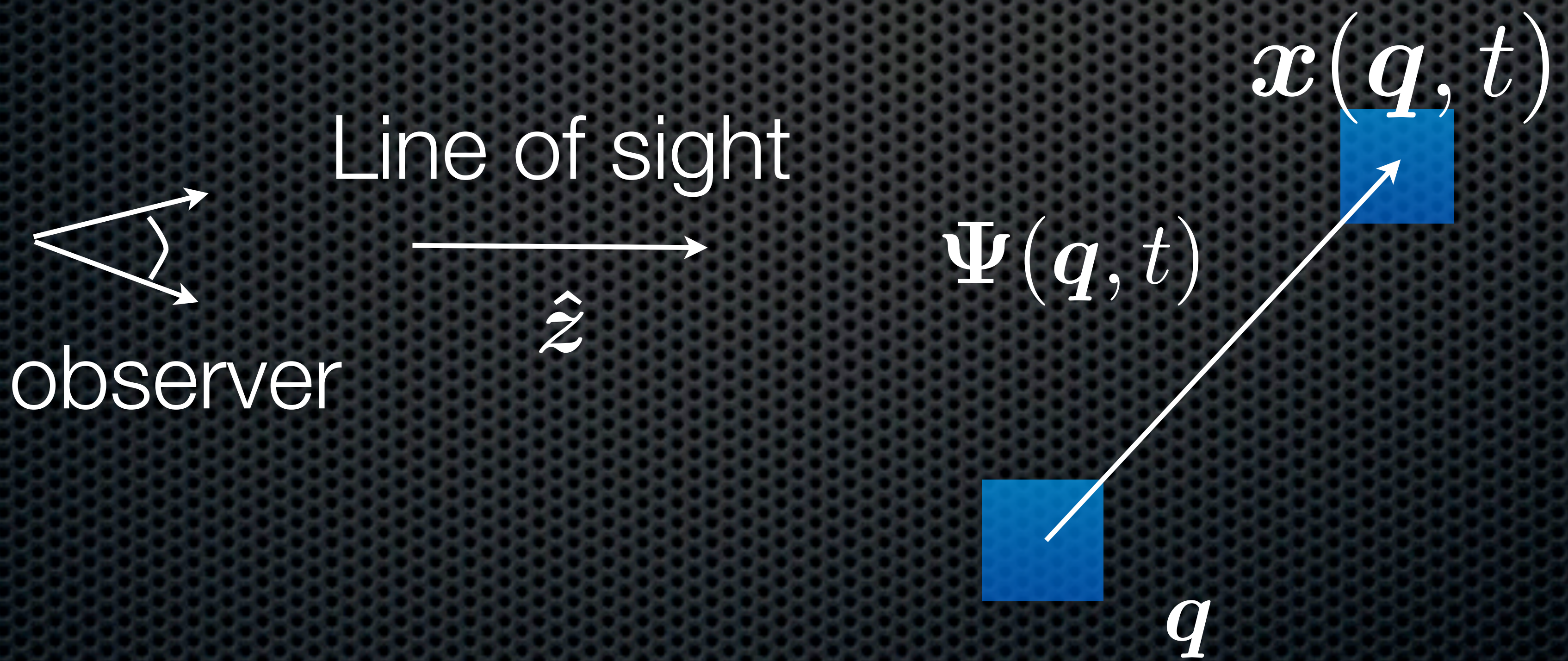

Redshift-space distortions

- Redshift-space distortions are easily incorporated into LRT
- Mapping is exactly linear in Lagrangian variables

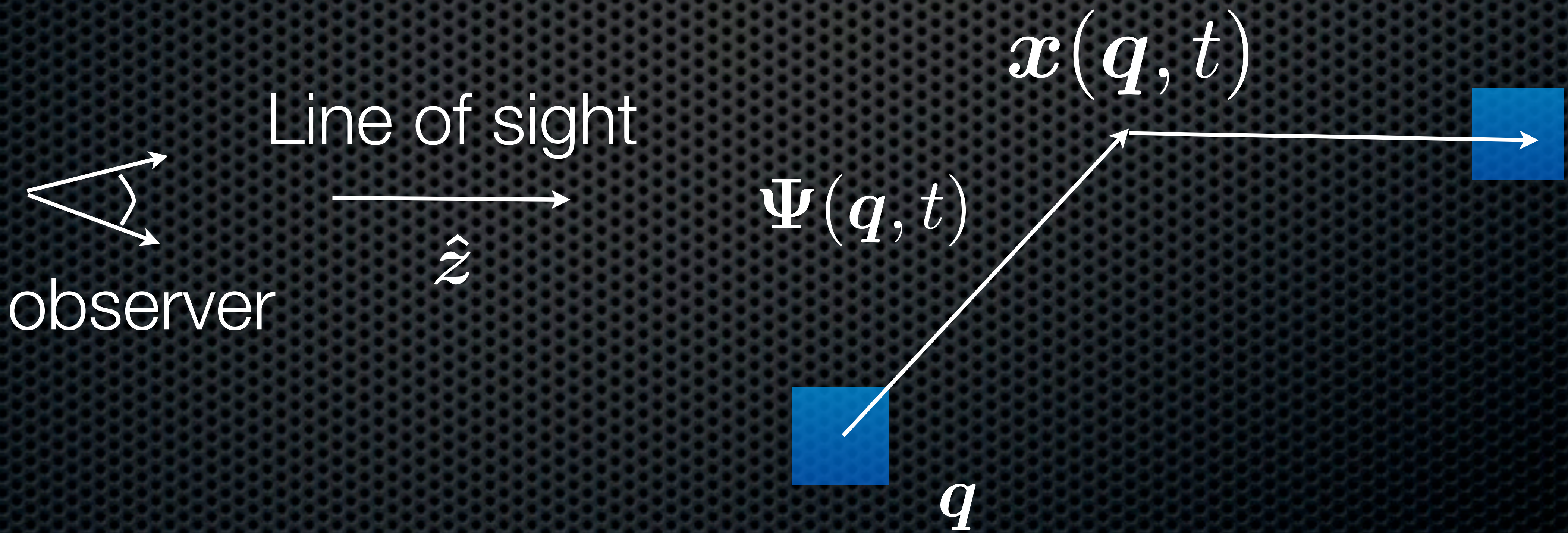

Redshift-space distortions

- Redshift-space distortions are easily incorporated into LRT
- Mapping is exactly linear in Lagrangian variables

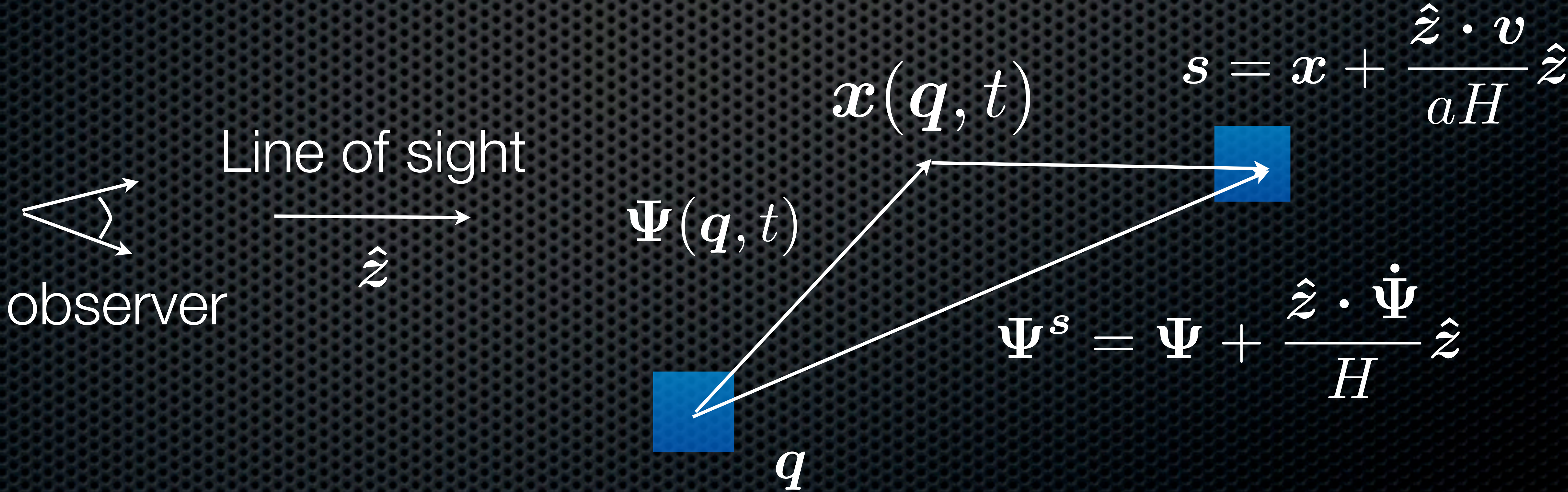

LRT with bias and redshift-space distortion

Matsubara 2008,2011

- The relation between Eulerian density field and Lagrangian variables

$$1+\delta_{\mathrm{X}}(\boldsymbol{x}) = \int d^3q [1+\delta^{\mathrm{L}}_{\mathrm{X}}(\boldsymbol{q})] \delta^3_{\mathrm{D}}[\boldsymbol{x}-\boldsymbol{q}-\boldsymbol{\Psi}(\boldsymbol{q})]$$

Biased Eulerian density field

Biased field in Lagrangian field

displacement(including redshift-space distortions)

- Perturbative expansion in Fourier space

kernel of the Lagrangian bias

$$\delta^{\mathrm{L}}_{\mathrm{X}}(\boldsymbol{k}) = \sum_{n=1}^{\infty} \frac{1}{n!} \int \frac{d^3k_1}{(2\pi)^3} \cdots \frac{d^3k_n}{(2\pi)^3} (2\pi)^3 \delta^3_{\mathrm{D}}(\boldsymbol{k}_{1\cdots n}-\boldsymbol{k}) b^{\mathrm{L}}_n(\boldsymbol{k}_1,\ldots,\boldsymbol{k}_n)\, \delta_{\mathrm{L}}(\boldsymbol{k}_1)\cdots\delta_{\mathrm{L}}(\boldsymbol{k}_n)$$

$$\tilde{\boldsymbol{\Psi}}(\boldsymbol{k}) = \sum_{n=1}^{\infty} \frac{i}{n!} \int \frac{d^3k_1}{(2\pi)^3} \cdots \frac{d^3k_n}{(2\pi)^3} (2\pi)^3 \delta^3_{\mathrm{D}}(\boldsymbol{k}_{1\cdots n}-\boldsymbol{k}) \boldsymbol{L}_n(\boldsymbol{k}_1,\ldots,\boldsymbol{k}_n) \delta_{\mathrm{L}}(\boldsymbol{k}_1)\cdots\delta_{\mathrm{L}}(\boldsymbol{k}_n)$$

Kernel of displacement(including redshift-space distortion)

Simulation parameters

WMAP7yr

Name	Ω_m	Ω_Λ	Ω_b	h	n_s	σ_8	L_{box}	N_p	z_{ini}	r_s	N_{run}
L1000(low resolution)	0.265	0.735	0.0448	0.71	0.963	0.80	$1000h^{-1}$Mpc	1024^3	36	$50h^{-1}$kpc	30
L500(high resolution)	0.265	0.735	0.0448	0.71	0.963	0.80	$500h^{-1}$Mpc	1024^3	42	$25h^{-1}$kpc	5

L1000(low resolution)				L500(high resolution)			
	$\bar{N}_h$	$\bar{n}_h[h^3\mathrm{Mpc}^{-3}]$	$\bar{M}_h[h^{-1}M_\odot]$		$\bar{N}_h$	$\bar{n}_h[h^3\mathrm{Mpc}^{-3}]$	$\bar{M}_h[h^{-1}M_\odot]$
$z=3$	4.00×10^5	4.00×10^{-4}	2.59×10^{12}	$z=3$	1.08×10^6	8.68×10^{-3}	4.58×10^{11}
$z=2$	1.21×10^6	1.21×10^{-3}	3.30×10^{12}	$z=2$	1.86×10^6	1.48×10^{-2}	6.12×10^{11}
$z=1$	2.38×10^6	2.38×10^{-3}	4.75×10^{12}	$z=1$	2.42×10^6	1.94×10^{-2}	9.07×10^{11}
$z=0.5$	2.82×10^6	2.82×10^{-3}	5.99×10^{12}	$z=0.5$	2.52×10^6	2.01×10^{-2}	1.15×10^{12}
$z=0.3$	2.93×10^6	2.93×10^{-3}	6.63×10^{12}	$z=0.3$	2.52×10^6	2.01×10^{-2}	1.27×10^{12}
$z=0$	3.05×10^6	3.05×10^{-3}	7.73×10^{12}	$z=0$	2.49×10^6	1.99×10^{-2}	1.47×10^{12}

- To compare the LRT predictions, we mainly use L1000 simulations whose number of particles are 1024^3, box size on a side is 1Gpc/h and number of realizations are 30.
  -> suitable for examining the BAOs accurately.

Mass function

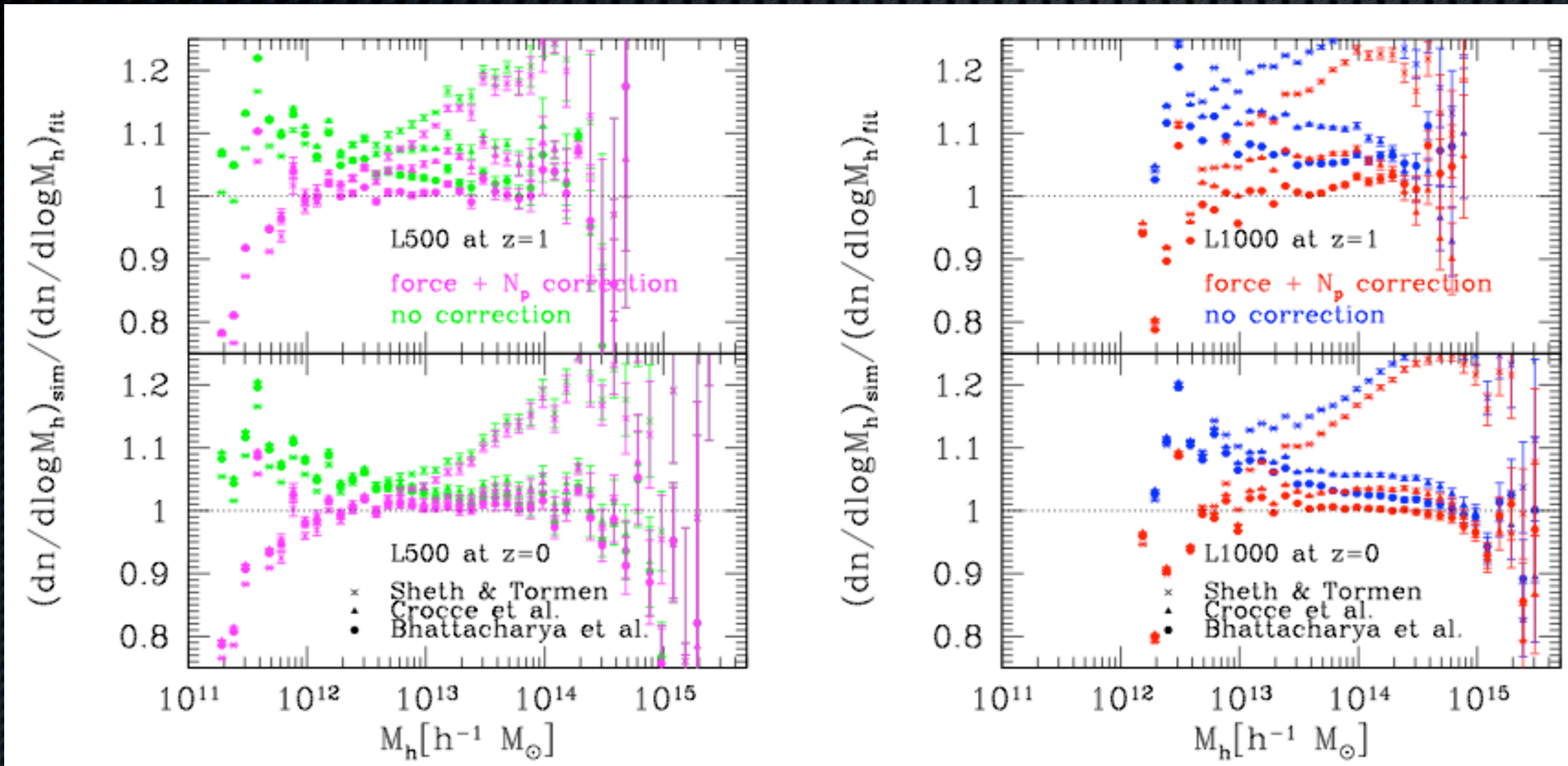

Our simulation results are supported by a recently proposed fitting formulae obtained by using large and high-resolution N-body simulations, such as Bhattacharya+(2011) and vice versa.

Mass function

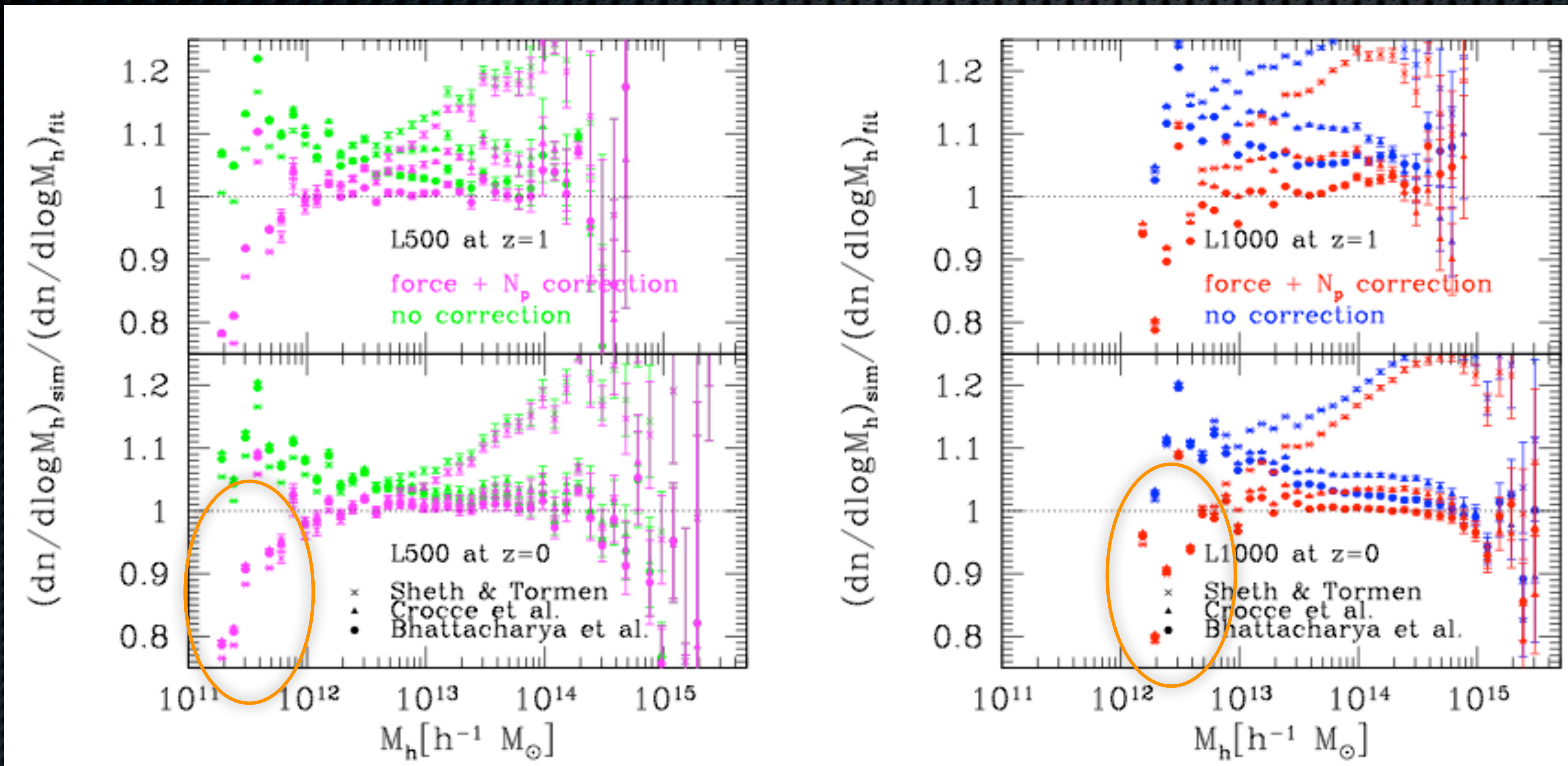

Deviation from unity shows that the FOF correction may not be perfect in haloes with small particles

Our simulation results are supported by a recently proposed fitting formulae obtained by using large and high-resolution N-body simulations, such as Bhattacharya+(2011) and vice versa.

Halo power spectra

$$P_{\rm hh,LRT}(k) = \exp\left[-k^2\sigma_{\rm v}^2\right]\left[(1+\langle F'\rangle)^2 P_{\rm L}(k) + E_{00}(k)\right]$$

$$P^{\rm s}_{\rm hh,LRT}(k,\mu) = \exp\left[-k^2\sigma_{\rm v}^2[1+f(f+2)\mu^2]\right]\left[(1+\langle F'\rangle + f\mu^2)^2 P_{\rm L}(k) + \sum_{n,m}\mu^{2n} f^m E_{nm}(k)\right]$$

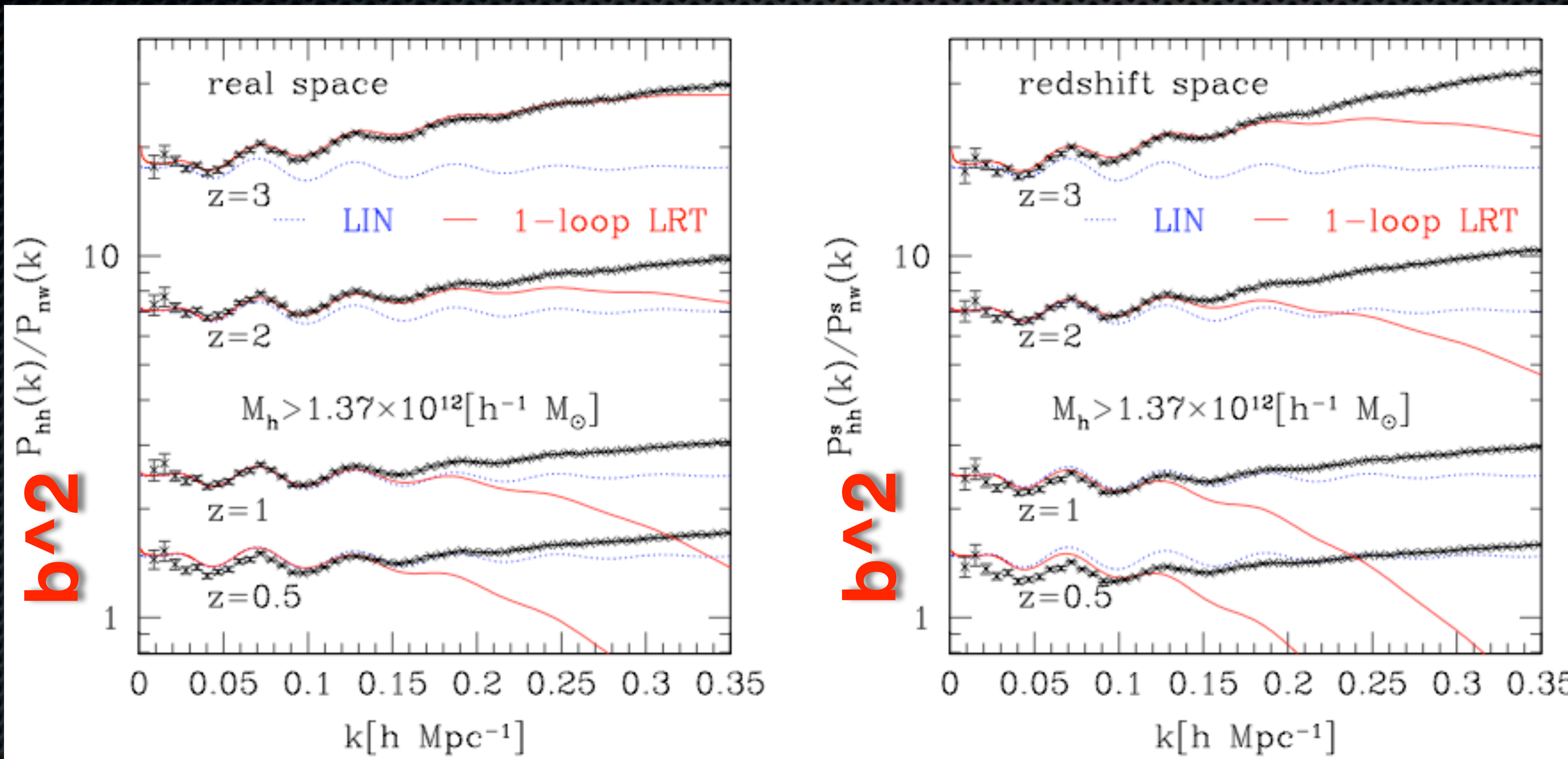

1-loop LRT agrees with simulation results on large scales in real and redshift space. As redshift is decreasing, the range of agreement is narrower because of nonlinearity of dynamics.

Halo power spectra

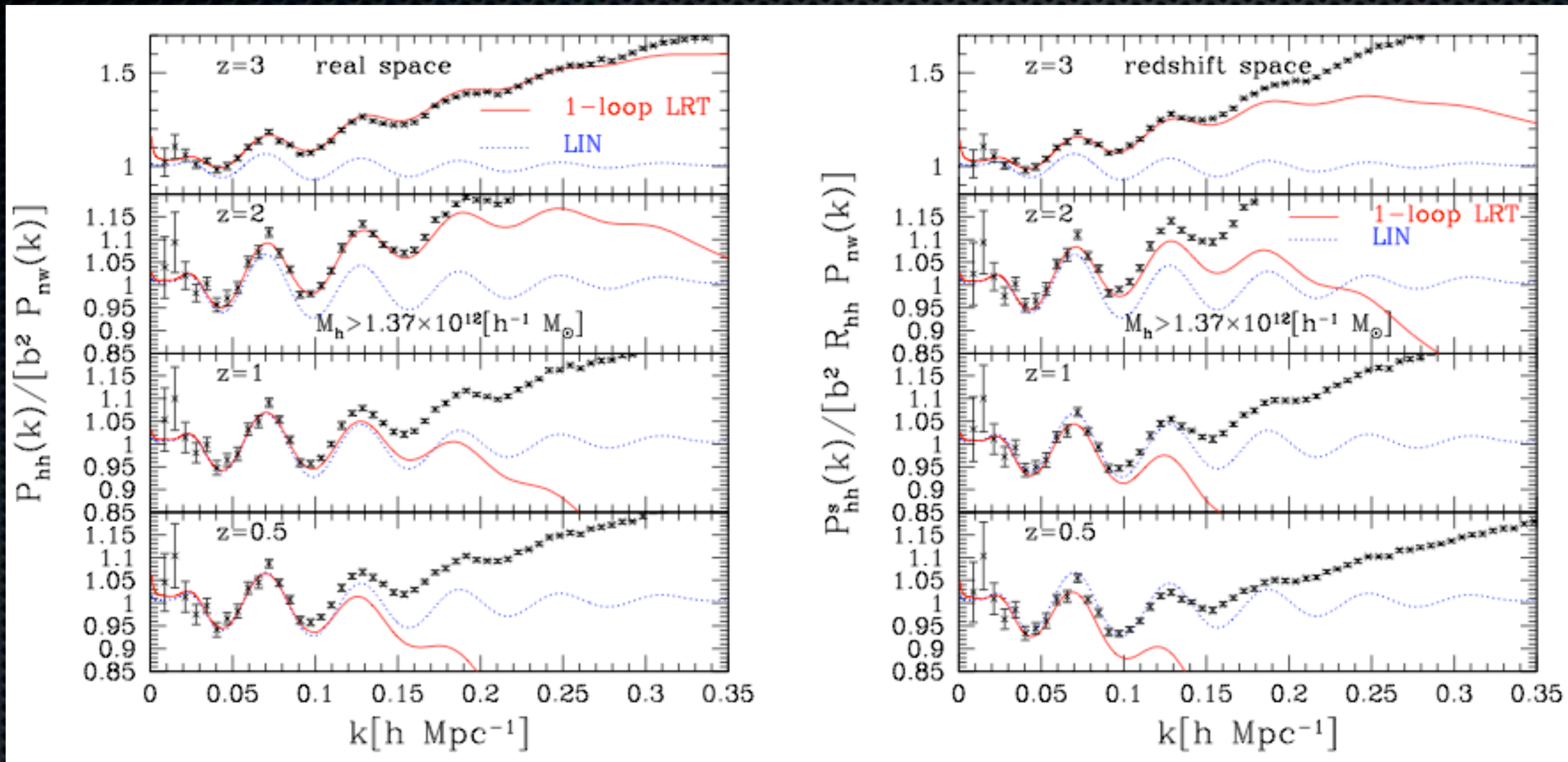

Same as previous figure, but vertical axis is divided by square of scale independent bias, b^2, to see more quantitatively.
The agreement in redshift-space is worse than that in real-space due to nonlinear redshift-space distortions.

Scale dependence of bias

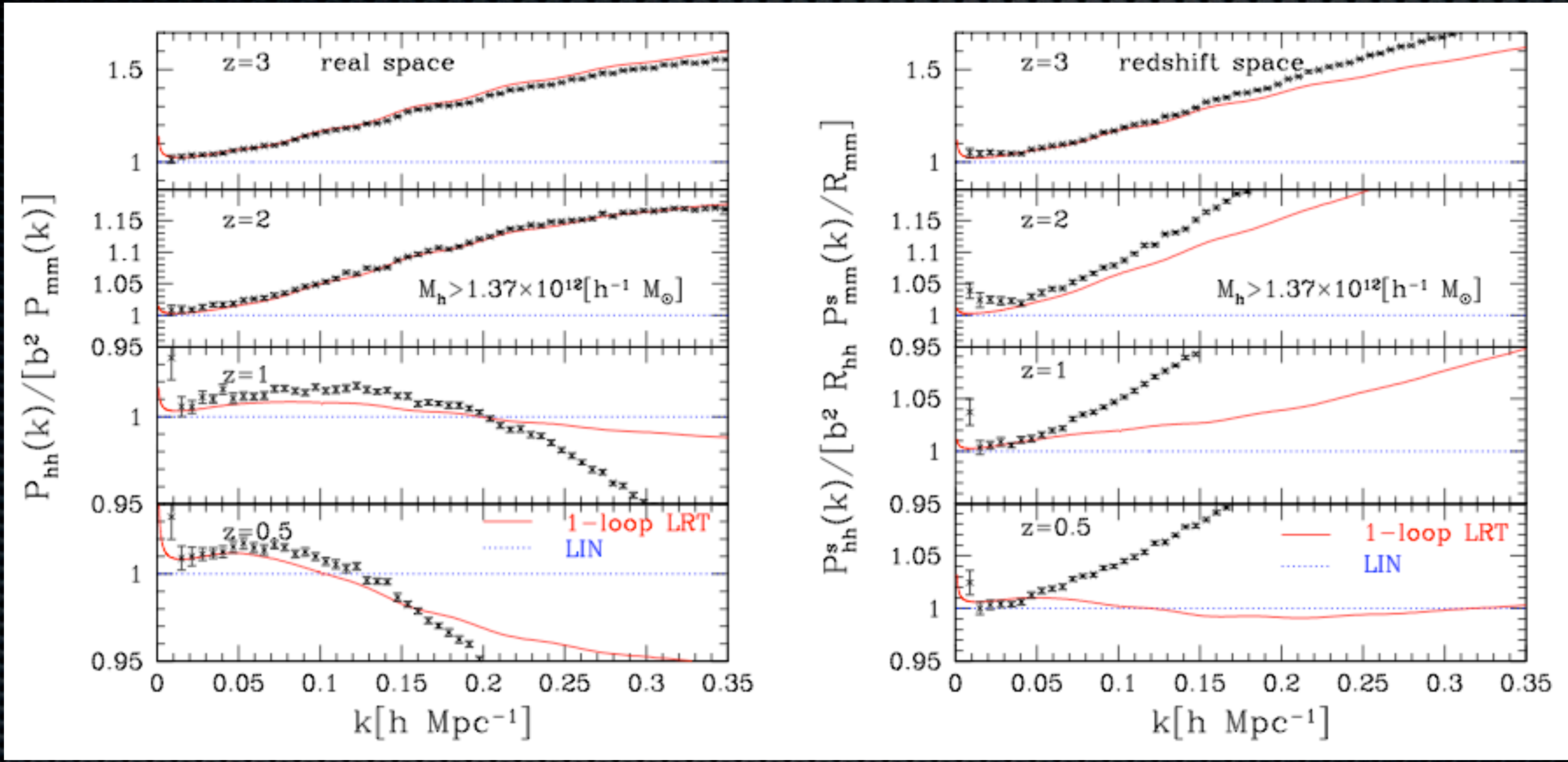

Same as previous figure, but Pnw is replaced with Pmm and Pmm^s that are corresponding matter power spectra, in order to get rid of nonlinearity of dynamics.

Therefore, the deviation from unity shows the nonlinearity of bias and that of bias and redshift-space distortions in real and redshift space.

Two-point correlation functions of haloes

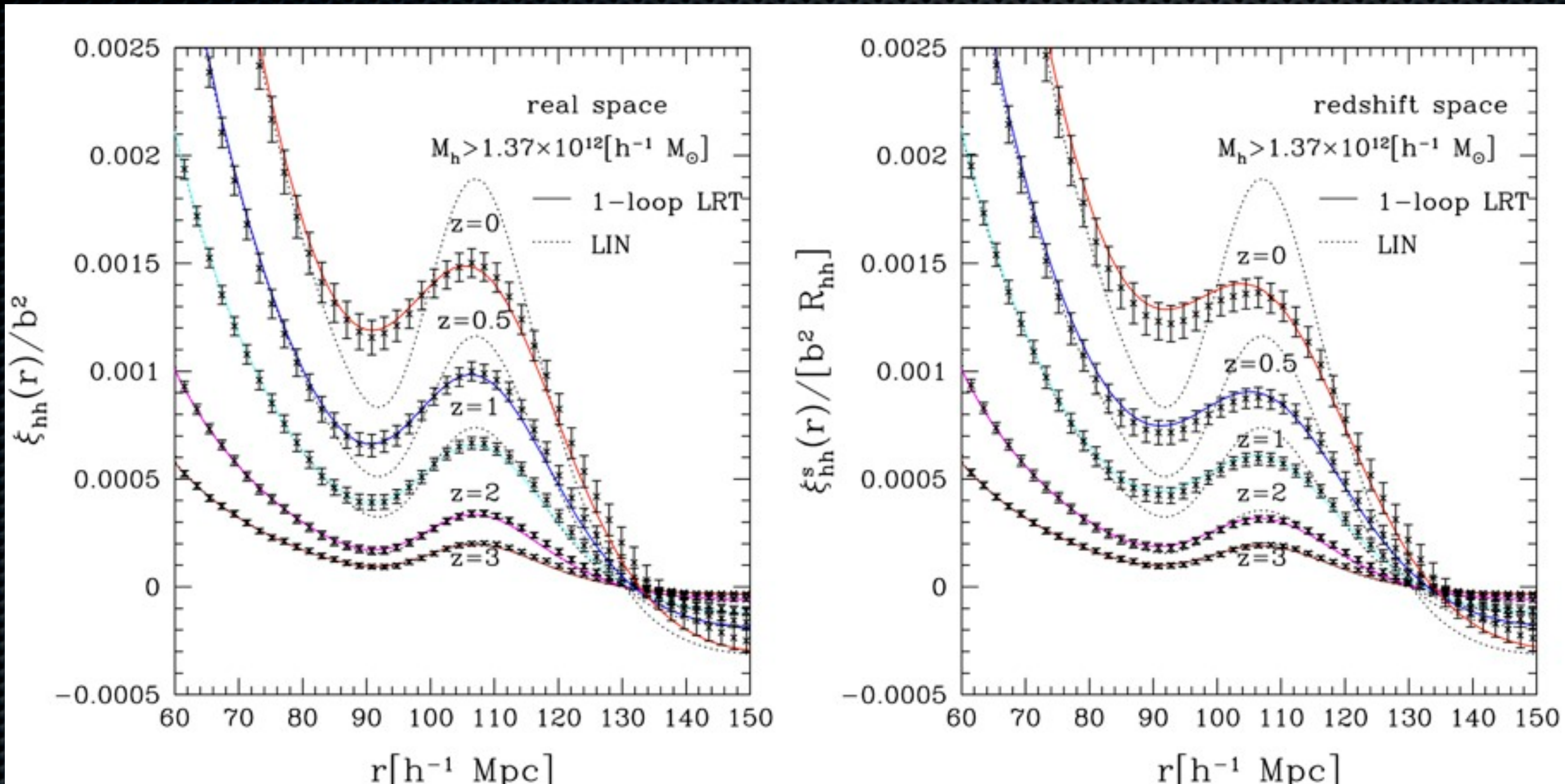

1-loop LRT well describes the acoustic peaks and nonlinear smearing effects both in real and redshift space.

Halo bias does not significantly change the shape of baryon peak.

Two-point correlation functions of matter

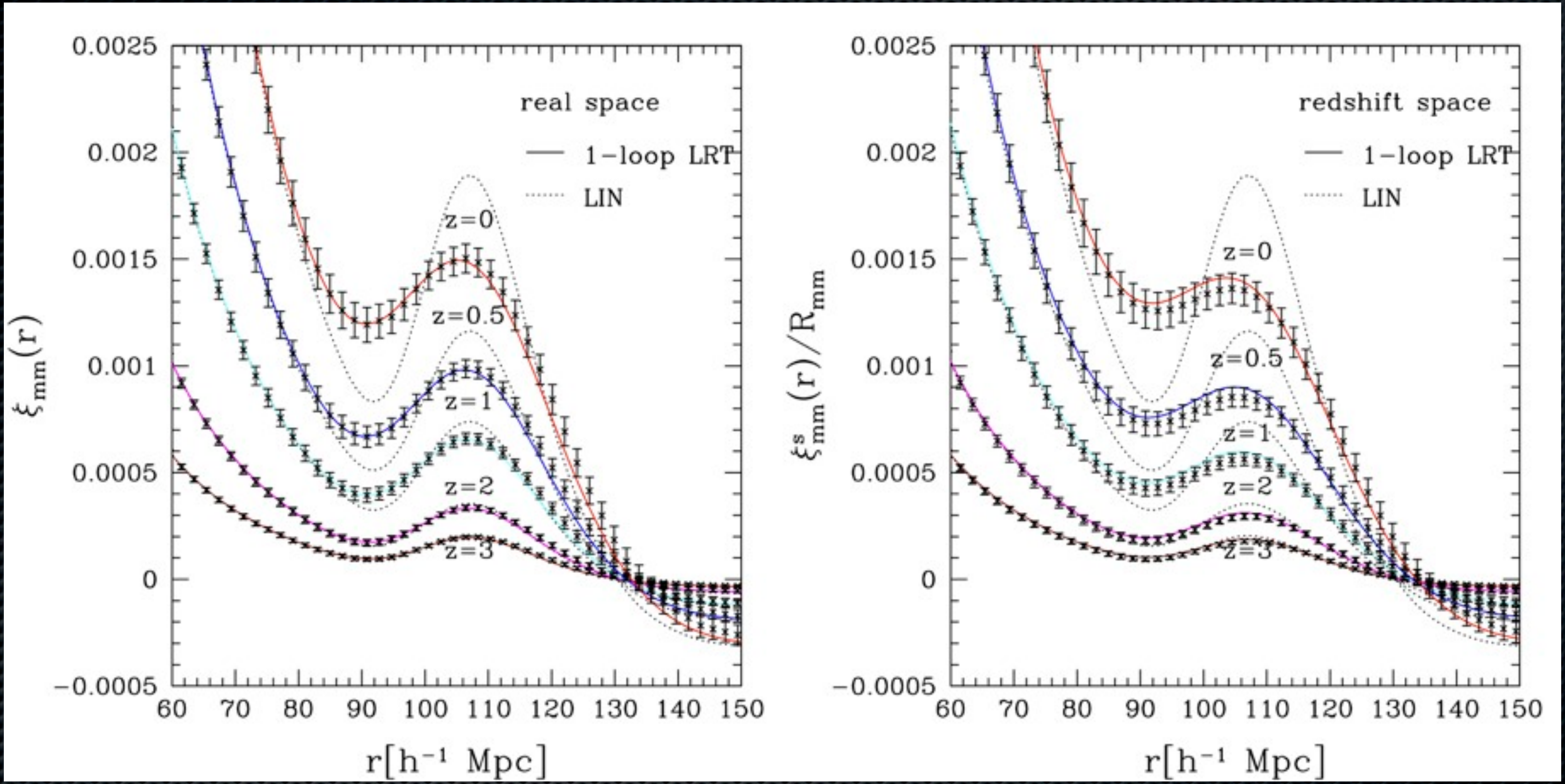

1-loop LRT well describes the acoustic peaks and nonlinear smearing effects both in real and redshift space.

Halo bias does not significantly change the shape of baryon peak.

Summary

- Advantage of Lagrangian resummation theory(LRT)
  - naturally incorporate halo bias and redshift-space distortions!
  - easier and faster to calculate the power spectrum than other resummation methods even in the presence of halo bias and redshift-space distortions.
- The power spectrum and correlation function of haloes from LRT well agree with N-body simulation results on scales of BAOs.
- Scale dependence of bias are well reproduced by LRT in real and redshift space, especially at high redshift.